# SIW Triplets Including Meander-Line and CRLH Resonators and Their Applications to Quasi-Elliptic Filters

Yilong Zhu, *Member, IEEE*, Yuandan Dong, *Senior Member, IEEE*, Jens Bornemann, *Life Fellow, IEEE*, Lin Gu, *Student Member, IEEE*, and Deisy Formiga Mamedes, *Member, IEEE*

***Abstract*— This article presents a design technique of quasi-elliptic filters by applying two novel planar triplets, which eliminates the need for negative couplings. A composite right-/left-handed (CRLH) resonator, together with a meander-line resonator, is investigated first in this article. These two resonators demonstrate a significant difference with respect to their phase shift characteristics that are completely opposite below and above their resonant frequencies. With such a feature, two meander-line and CRLH-loaded substrate integrated waveguide (SIW) triplets are proposed, which can produce a transmission zero (TZ) above and below the passbands if an inductive cross coupling is applied. Therefore, all couplings would be positive regardless of the location of TZs. The applications of the two triplets to quasi-elliptic filters, which are realized by parallel and cascaded triplet topologies, are then illustrated. Two filter prototypes operating at the *X*-band are designed and fabricated for validation. They show outstanding electrical performance in terms of high selectivity, low loss, and compactness. It indicates that a joint application of conventional shunt *LC* resonant nodes and a CRLH node is a viable option in filter design.**

***Index Terms*— Composite right-/left-handed (CRLH) resonator, meander-line resonator, phase shift characteristics, quasi-elliptic filters, substrate integrated waveguide (SIW) triplets, transmission zero (TZ).**

## I. Introduction

QUASI-ELLIPTIC bandpass filters, which present sharp roll-off and high selectivity with finite transmission zeros (TZs), have been in increasing demand in areas of mobile and satellite communication in order to suppress interferences from adjacent frequency bands, especially for overcrowded bands in commercial applications [1], [2]. To improve the steepness of passband edges, a common method is to place TZs at both sides of passbands.

Numerous techniques have been introduced to generate TZs, including, but not limited to, extracted-pole techniques [3], [4], [5], [6], [7], [8], [9], [10], mixed electric and magnetic couplings [11], [12], [13], [14], [15], [16], bypass couplings [17], [18], [19], [20], [21], [22], [23], and cross couplings [24], [25], [26], [27], [28], [29], [30]. The extracted-pole technique is an emerging method to introduce TZs, which has been developing in terms of single-/dual-band filter synthesis using extracted-pole sections [9], [10]. This technique shows merit to create TZs with inline filter configurations [3], [4], [5], [6], [7]. As for mixed electric and magnetic couplings, which are also interpreted as frequency-dependent couplings (FDCs) [12], [13], [14], [15], they are able to create a TZ in the lower stopband when FDC is capacitively dominant or in the upper stopband when it is inductively dominant [16]. As for bypass couplings, they are realized by overmoded cavities [17]. Although it provides an alternative method to generate TZs, some drawbacks are inevitable, such as enlarged size [18], [19], [20] and spurious bands below passbands [21]. An appropriate application of this technique is to design THz components, in which large dimensions are sometimes preferred due to the higher standard fabrication process [22], [23]. On the other hand, it has been the most popular way to create TZs by utilizing cross couplings [24]. For example, a TZ can be created either below or above the passband if the cross coupling is capacitive (negative) or inductive (positive) in a triplet topology [25], [26]; a TZ would be located at both sides of the passband if a negative cross coupling exists in a quadruplet topology [27]. It is noted that the requirement of negative couplings is significantly essential for TZs' generation in cross-coupled filters.

For practical implementation of negative cross couplings, especially in waveguide filters, they are often realized by capacitive irises in rectangular waveguide filters [28] or realized by diagonal capacitive probes [29] and rotated resonators [30], [31] in combline filters. Compared with positive couplings implemented by inductive irises, it would be more costly and complicated to realize capacitive couplings. Alternatively, a simple and economical planar waveguide, which is known as substrate integrated waveguide (SIW), can be used. A typical way to achieve negative couplings in SIW filters is to form electric-coupling structures between

Manuscript received 21 July 2022; accepted 18 November 2022. Date of publication 8 December 2022; date of current version 5 May 2023. This work was supported by the Natural Sciences and Engineering Research Council (NSERC) of Canada. The work of Yilong Zhu was supported by the China Scholarship Council (CSC) under Grant 202006070154. *(Corresponding author: Yuandan Dong.)*

Yilong Zhu is with the School of Electronic Science and Engineering, University of Electronic Science and Technology of China, Chengdu 611731, China, and also with the Department of Electrical and Computer Engineering, University of Victoria, Victoria, BC V8W 2Y2, Canada.

Yuandan Dong and Lin Gu are with the School of Electronic Science and Engineering, University of Electronic Science and Technology of China, Chengdu 611731, China (e-mail: ydong@uestc.edu.cn).

Jens Bornemann and Deisy Formiga Mamedes are with the Department of Electrical and Computer Engineering, University of Victoria, Victoria, BC V8W 2Y2, Canada (e-mail: j.bornemann@ieee.org).

Color versions of one or more figures in this article are available at https://doi.org/10.1109/TMTT.2022.3225447.

Digital Object Identifier 10.1109/TMTT.2022.3225447

nonadjacent cavities, such as S-shape slots in [32], a coplanar line in [33], an H-shape slot in [34], and an interdigital-like capacitive unit in [35]. However, these structures would lead to degraded unloaded quality factors ($Q_u$) caused by radiation effects. Moreover, folded filter configurations are required to construct quadruplet coupling topologies. By using multilayer substrates, negative couplings can also be introduced without radiation loss. For example, a typical way to realize negative couplings is to etch a circular aperture on the layer interface [36]. In [37], a V-shape structure was proposed, which is placed inside the SIW cavities. Based on an air-filled SIW platform, a negative coupling is realized by an SIW transmission line with a 180° phase shift [38]. Although these structures are able to create negative couplings with good self-packaged characteristics, it is always more expensive and complicated to design and fabricate filters on multilayer substrates.

Instead of using negative couplings to generate a TZ below the passband in a triplet topology or a TZ at both sides of the passband in a quadruplet, this article presents a design technique of quasi-elliptic filters using all inductive couplings. It is achieved by a joint implementation of right-handed (RH) and composite right-/left-handed (CRLH) resonators, whose phase characteristics are completely opposite below and above their resonant frequencies. With such a feature, two novel meander-line- and CRLH-based SIW triplets are investigated first, which can generate a TZ below and above the passband, respectively. A circuit-based analysis process is illustrated, including resonance and transfer characteristics, generation of TZs, and filter synthesis. Two filter prototypes with quasi-elliptic responses are designed and fabricated for demonstration. Compared with the filters using negative coupling structures in [32], [33], [34], [35], [36], and [37], this work presents the following merits/novelty.

1) All couplings are inductive; thus, negative coupling structures are not required anymore. Since the CRLH resonator presents a reversed phase shift performance compared with conventional RH resonators, a negative cross coupling can be replaced by an inductive coupling to achieve identical TZ positions. Therefore, instead of using negative-coupling structures, all couplings can be realized by inductive irises.

2) A new filter design technique combining a CRLH resonant node with conventional shunt *LC* nodes is investigated for the first time, which shows advantages in the generation and controllability of TZs without negative cross couplings.

3) *Miniaturization:* Compared with SIW cavities, microstrip-based meander-line and CRLH resonators present smaller sizes. Miniaturized filters can be realized by using hybrid SIW and microstrip structures while maintaining a moderate $Q_u$.

The rest of this article is organized as follows. In Section II, the resonance and transfer characteristics of the meander-line and CRLH resonators are investigated. Subsequently, two SIW triplets formed by these two resonators are then discussed in terms of their TZ behaviors in Section III. Next, their applications to quasi-elliptic filters by using two different triplet topologies are presented in Section IV. Finally, a comparison and conclusion are presented in Sections V and VI.

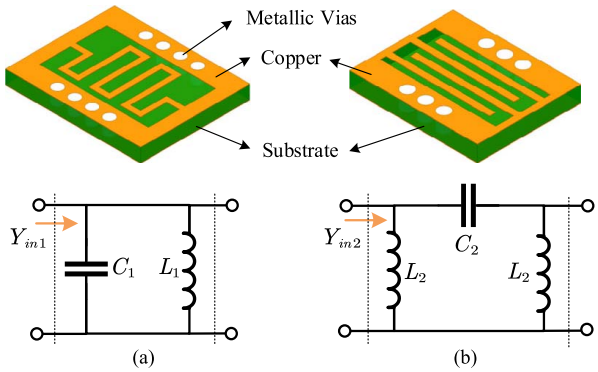


Fig. 1. (a) Meander-line resonator and its equivalent circuit. (b) CRLH resonator and its equivalent circuit.

## II. Meander-Line and CRLH Resonators

Due to the miniaturized size, meander-line resonators have been widely used in filter designs, especially for high-temperature superconductor (HTS) filters [39], [40], [41]. Various HTS filter applications, including quasi-elliptic [39], multiband [40], and wide-stopband [41] filters, have been developed. On the other hand, CRLH resonators, which are also characterized by miniaturization, are mostly realized by mushrooms [42], [43] and interdigital structures [44], [45]. The left-handed (or series) capacitance is significantly dominant among these structures, while, for meander-line resonators, the RH inductance is dominant. Although meander-line and CRLH resonators, and their application to advanced SIW filters, such as meander-line-based filters in [46] and CRLH-based filters in [45] and [47], have been extensively studied, a comprehensive and comparative investigation of the two resonators is still missing, especially a deep exploration of their electrical performance. Therefore, in this section, an exhaustive study of the two resonators is performed in terms of their resonance and transfer characteristics, and a joint application of these two types of resonators, i.e., the conventional resonant nodes and a CRLH node, is first presented in this article.

### A. Resonance Characteristics

Fig. 1(a) and (b) shows the proposed meander-line [48] and CRLH resonators [49], respectively. The meander-line resonator is realized by etching a meander line on the top metal layer of the substrate, surrounded by a pair of via arrays. For the CRLH resonator, an interdigital structure is etched on the top. It is well known that the meander-line resonator is a type of conventional resonant node, which can be equivalent to a parallel *LC* circuit, as shown in Fig. 1(a). As for the CRLH resonator, since the series capacitance among the electrodes is more dominant than the grounded capacitance, its simplified equivalent circuit can be considered as a $\pi$-type *LC* circuit in Fig. 1(b), in which the shunt inductors ($L_2$) are introduced by the metallic-via arrays.

For the two resonant circuits, their input admittance can be derived as

$$Y_{\text{in1}} = \frac{1}{j\omega L_1} + j\omega C_1 = \frac{1-\omega^2 L_1 C_1}{j\omega L_1} \tag{1}$$

$$Y_{\text{in2}} = \frac{1}{j\omega L_2} + \frac{1}{\frac{1}{j\omega C_2} + j\omega L_2} = \frac{1-2\omega^2 L_2 C_2}{j\omega L_2\left(1-\omega^2 L_2 C_2\right)}. \tag{2}$$

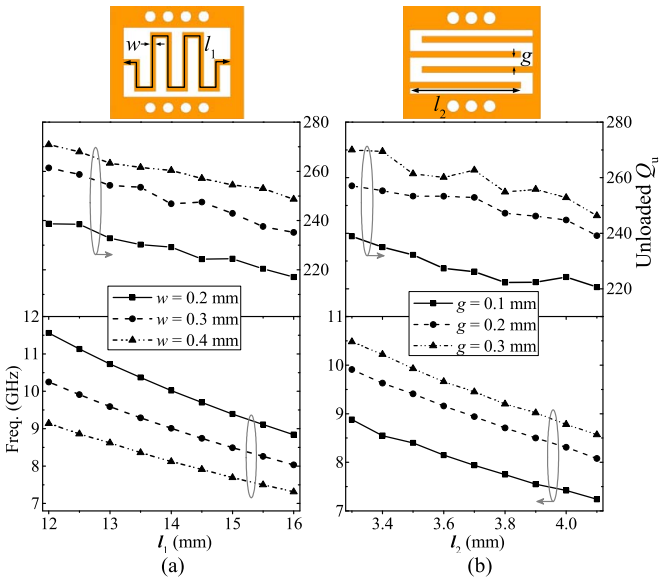


Fig. 2. (a) Extracted resonant frequencies and unloaded quality factors of the meander-line resonator versus $l_1$ with $w$ as a variable. (b) Extracted resonant frequencies and unloaded quality factors of the CRLH resonator versus $l_2$ with $g$ as a variable.

When the imaginary parts of the input admittances vanish, namely, $\mathrm{im}(Y_{\mathrm{in1}}) = \mathrm{im}(Y_{\mathrm{in2}}) = 0$, the resonant frequencies of the two circuits can be calculated as

$$\omega_1 = \sqrt{\frac{1}{L_1 C_1}} \tag{3}$$

$$\omega_2 = \sqrt{\frac{1}{2L_2 C_2}}. \tag{4}$$

Thus, both the resonant frequencies are determined by the inductance and capacitance of the circuit components.

To further explore the resonant characteristics of the two resonators, the impact of varying dimensions is investigated. The extracted resonant frequencies and unloaded quality factors ($Q_u$) in Fig. 2 are obtained by eigenmode simulations. For the meander-line resonator, Fig. 2(a) shows that the resonant frequency decreases with increasing line length $l_1$ if the linewidth $w$ is fixed, and $Q_u$ presents a similar tendency but with a flatter curve. Inversely, if $l_1$ is fixed, the wider linewidth $w$ leads to lower resonant frequencies and higher $Q_u$. As for the CRLH resonator [see Fig. 2(b)], the length ($l_2$) and the gap ($g$) of the electrodes are investigated. The resonant frequency decreases with increasing $l_2$, and the unloaded quality factor shows a similar tendency. As for the gap of the electrodes, a wider gap $g$, which means a reduced series capacitance, can increase the resonant frequency and enhance $Q_u$.

### *B. Transfer Characteristics*

To study the transfer characteristics of the two resonators, a typical circuit-based analysis method is applied. As shown in Fig. 3, two voltage sources with internal resistance are used to feed the two resonators, respectively. The output voltages are taken across the inductors $L_1$ and $L_2$, respectively.

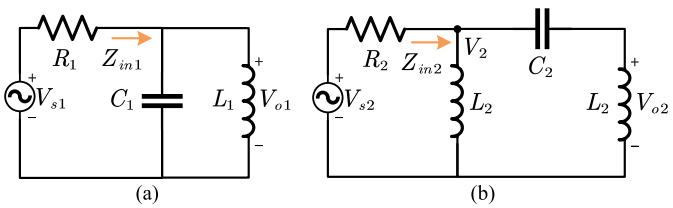


Fig. 3. (a) Meander-line resonator fed by a voltage source with the internal resistance of $R_1$. (b) CRLH resonator fed by a voltage source with the internal resistance of $R_2$.

For the first circuit shown in Fig. 3(a), its transfer function can then be obtained as

$$H_1(\omega) = \frac{Z_{\mathrm{in1}}}{Z_{\mathrm{in1}} + R_1} = \frac{j\omega L_1}{j\omega L_1 + R_1\left(1 - \omega^2 L_1 C_1\right)}. \tag{5}$$

To simplify the derivation, a weak feeding condition is considered here, namely, $R_1 \gg \omega_1 L_1$. Consequently, the simplified transfer function can be deduced by neglecting $j\omega L_1$ in the denominator

$$H_1(\omega) = \frac{j\omega L_1}{R_1\left(1 - \omega^2 L_1 C_1\right)}. \tag{6}$$

Therefore, the amplitude and phase functions can be approximated as

$$|H_1(\omega)| = \frac{\omega L_1}{\left|R_1\left(1 - \omega^2 L_1 C_1\right)\right|} \tag{7}$$

$$\varphi_1 = \begin{cases} +90^\circ, & \text{when } \omega < \omega_1 \\ 0, & \text{when } \omega = 0 \\ -90^\circ, & \text{when } \omega > \omega_1. \end{cases} \tag{8}$$

Equation (7) also indicates that the resonant frequency of the first resonator is, at which the maximum amplitude response can be achieved. According to (8), there is a $+90^\circ$ phase shift below the resonance and $-90^\circ$ above the resonance, which is consistent with the description in [47].

As for the second circuit shown in Fig. 3(b), the input impedance of the resonator ($Z_{\mathrm{in2}}$) can be derived from (2)

$$Z_{\mathrm{in}\,2} = \frac{1}{Y_{\mathrm{in}\,2}} = \frac{j\omega L_2 \cdot \left(1 - \omega^2 L_2 C_2\right)}{1 - 2\omega^2 L_2 C_2}. \tag{9}$$

The input voltage to the resonator can then be calculated as

$$\begin{aligned} V_2 &= \frac{Z_{\mathrm{in2}}}{Z_{\mathrm{in2}} + R_2} V_s \\ &= \frac{j\omega L_2 \cdot \left(1 - \omega^2 L_2 C_2\right)}{j\omega L_2 \cdot \left(1 - \omega^2 L_2 C_2\right) + R_2\left(1 - 2\omega^2 L_2 C_2\right)} V_s. \end{aligned} \tag{10}$$

Thus, the output voltage is obtained as

$$\begin{aligned} V_{o2} &= \frac{j\omega L_2}{j\omega L_2 + \frac{1}{j\omega C_2}} V_2 \\ &= \frac{-j\omega L_2 \cdot \omega^2 L_2 C_2}{j\omega L_2 \cdot \left(1 - \omega^2 L_2 C_2\right) + R_2\left(1 - 2\omega^2 L_2 C_2\right)} V_s. \end{aligned} \tag{11}$$

Therefore, the transfer function of the second circuit can be represented as

$$H_2(\omega) = \frac{V_{o2}}{V_{s2}} = \frac{-j\omega L_2 \cdot \omega^2 L_2 C_2}{j\omega L_2 \cdot \left(1 - \omega^2 L_2 C_2\right) + R_2\left(1 - 2\omega^2 L_2 C_2\right)}. \tag{12}$$

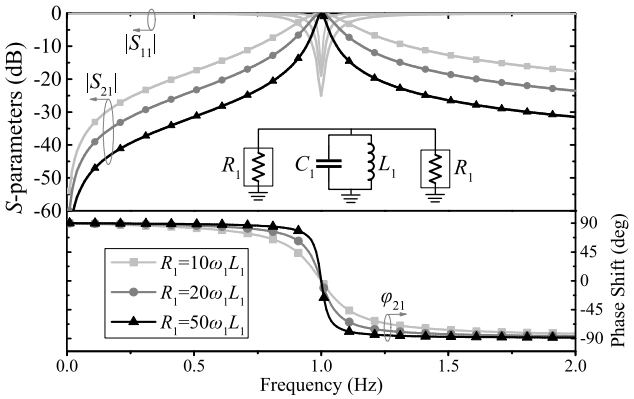


Fig. 4. Simulated transfer responses of the meander-line resonator and circuit schematic ($L_1 = 1/2\pi$ H and $C_1 = 1/2\pi$ F).

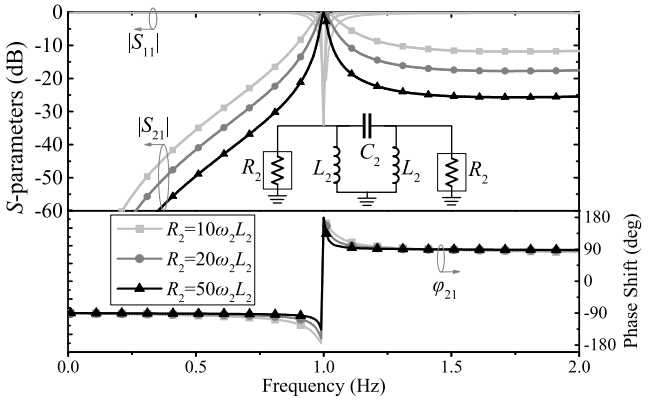


Fig. 5. Simulated transfer responses of the CRLH resonator and circuit schematic ($L_2 = 1/2\pi$ H and $C_2 = 1/4\pi$ F).

Similarly, under the weak feeding condition ($R_2 \gg \omega_2 L_2$), the term $j\omega L_2(1 - \omega^2 L_2 C_2)$ can be neglected, and (12) is simplified as

$$H_2(\omega) = \frac{-j\omega L_2 \cdot \omega^2 L_2 C_2}{R_2\left(1 - 2\omega^2 L_2 C_2\right)}. \tag{13}$$

Hence, the amplitude and phase functions can be obtained as

$$|H_2(\omega)| = \frac{\omega L_2 \cdot \omega^2 L_2 C_2}{\left|R_2\left(1 - 2\omega^2 L_2 C_2\right)\right|} \tag{14}$$

$$\varphi_2 = \begin{cases} -90^\circ, & \text{when } \omega < \omega_2 \\ 0, & \text{when } \omega = 0 \\ +90^\circ, & \text{whe } \omega > \omega_2. \end{cases} \tag{15}$$

Equation (14) indicates that the resonant frequency of the circuit is $\omega_2 = \sqrt{1/2\,L_2 C_2}$, which is consistent with (4). In addition, according to (15), the phase shift is found to be $-90^\circ$ below the resonance and $+90^\circ$ above the resonance. Compared with the first resonator, the second resonator shows a completely reversed phase response below and above its resonant frequency.

To verify the above conclusions, an analysis procedure based on circuit simulation is performed. For the first (meander-line) resonant circuit, the simulated amplitude and phase responses are depicted in Fig. 4, in which the circuit schematic is also shown. For simplicity, the resonant frequency is set at 1 Hz. To realize the weak feeding condition of $R_1 \gg \omega_1 L_1$, three different levels of internal impedance are arranged, as shown in Fig. 4. It can be observed that the bandwidth becomes wider with lower internal impedance, but the out-of-band rejection would be degraded as well. In terms of the phase shift, it tends to be $+90^\circ$ below and $-90^\circ$ above the resonance, corresponding to the theoretical derivations. Fig. 5 depicts the transfer responses of the CRLH resonant circuit. Similarly, the small internal impedance contributes to the wide bandwidth and decreased out-of-band rejection. As opposed to the first circuit, the phase shift is found to be $-90^\circ$ below the passband and $+90^\circ$ above the passband. It is worth noting that, for both of the two circuits, the phase curves would be sharper near the resonance if the internal impedance increases.

Furthermore, the two electromagnetic (EM) models, namely, the meander-line and CRLH resonators, are investigated to

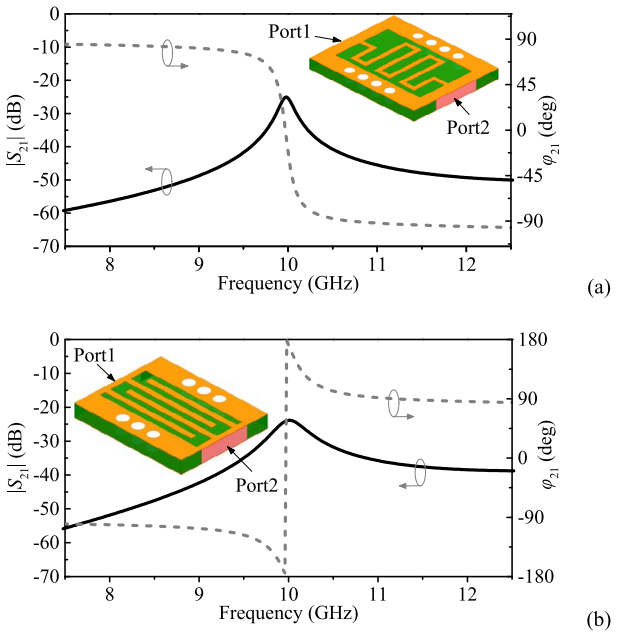


Fig. 6. (a) Simulated transfer responses of the meander-line resonator with EM model inset. (b) Simulated transfer responses of the CRLH resonator with EM model inset. (The internal impedance of the feeding ports is defined at 2 kΩ.)

demonstrate the above conclusions. Fig. 6(a) and (b) shows the EM-simulated amplitude and phase responses of the two resonators under the weak feeding condition. For the meander-line resonator, $+90^\circ$ phase shift is observed below the passband, while it is $-90^\circ$ above the passband. On contrary, $-90^\circ$ phase shift below the passband is generated for the CRLH resonator, and it is $+90^\circ$ above the passband. These observations reflect consistency with the theoretical and circuit-based results.

To summarize, this section presents an important fact that the CRLH resonator displays a totally inversed phase shift characteristic compared to conventional shunt *LC* resonators. For the CRLH resonator, the phase shift tends toward $-90^\circ$ below and $+90^\circ$ above the resonance, while, for conventional resonators, it is $+90^\circ$ below and $-90^\circ$ above the resonance. This converse phase behavior would lead to different generations of TZs if we apply these two types of resonators

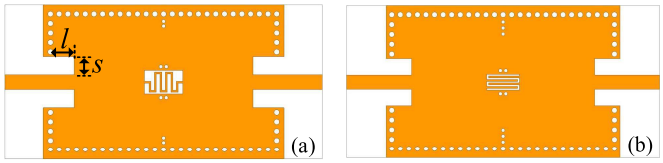


Fig. 7. (a) First SIW triplet formed by adding a meander-line resonator. (b) Second triplet formed by adding a CRLH resonator.

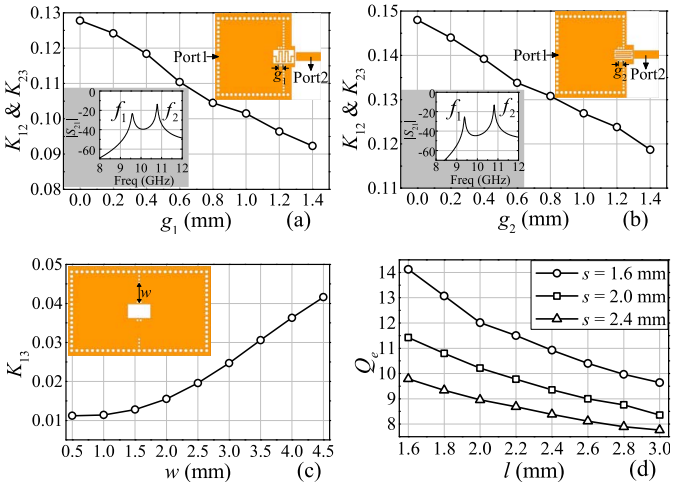


Fig. 8. Extracted coupling coefficients between (a) SIW cavity and meander-line resonator, (b) SIW cavity and CRLH resonator, and (c) two SIW cavities. (d) Extracted external quality factors.

to filter designs. Therefore, Sections III and IV present two SIW triplets based on the proposed resonators.

## III. Two SIW Triplets

Two SIW triplets formed by adding the meander-line and CRLH resonators to a two-cavity SIW filter are presented in Fig. 7(a) and (b), respectively. For the first triplet, two metallic-via arrays are placed around the meander-line resonator to adjust the couplings between the SIW and microstrip resonators. A pair of symmetric coupling windows is constructed between the two SIW cavities, which are utilized to create the cross coupling. For the second SIW triplet shown in Fig. 7(b), the CRLH resonator is etched in the center instead with an inductive cross coupling introduced as well.

Fig. 8(a) and (b) shows the extracted coupling coefficients between the SIW cavity and the meander-line/CRLH resonators. It is seen that the coupling coefficients are mainly controlled by the dimensions of the metallic-via arrays ($g_1$ and $g_2$), and they show a declining tendency when $g_1$ and $g_2$ increase from 0 to 1.4 mm. Fig. 8(c) depicts the simulated cross-coupling coefficient between the SIW cavities, which increases from 0.0112 to 0.0416 when the width of the inductive windows ($w$) increases from 0.5 to 4.5 mm. As for the external quality factors ($Q_e$), they can be determined by the size of the feeding slots ($l$ and $s$). As presented in Fig. 8(d), the extracted $Q_e$ decreases with the increased slot length ($l$), which means that more energy can be coupled into the SIW cavity. In addition, the slot width ($s$) also shows a significant impact on the external quality factors, and wider $s$ leads to a smaller $Q_e$.

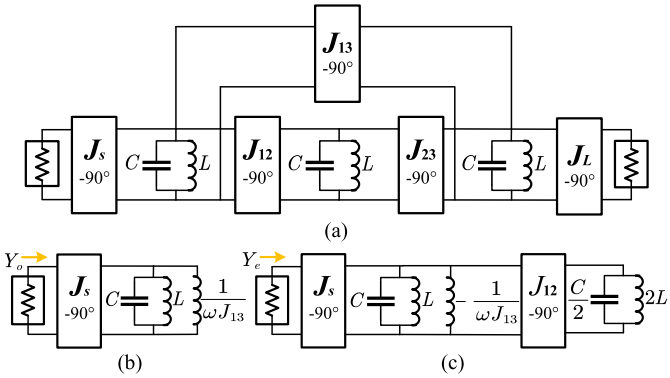


Fig. 9. (a) Network circuit representation of the first SIW triplet. (b) Its odd-mode and (c) even-mode equivalent circuits.

### A. Analysis of the First SIW Triplet

By using network circuit methods, the first SIW triplet is equivalent to the circuit shown in Fig. 9(a), in which all the resonators are represented by shunt $LC$ pairs. $J$ inverters with phase shifts of $-90°$ can be used to implement couplings between any two resonators. The couplings would be inductive if $J > 0$ or capacitive if $J < 0$. Note the $J$ inverter ($J_{13}$) acts as a cross coupling between the nonadjacent resonators. To analyze this circuit, the odd- and even-mode decompositions of the circuit are depicted in Fig. 9(b) and (c), respectively.

Assuming that the input admittance of the parallel $LC$ pairs is represented by $Y_P$, according to (1), $Y_P$ can be derived as

$$Y_P = j\frac{\omega^2 LC - 1}{\omega L}. \tag{16}$$

Therefore, the input admittances of the odd- and even-mode circuits can be obtained as

$$Y_o = \frac{J_s^2}{Y_P - jJ_{13}}, \quad Y_e = \frac{J_s^2}{\frac{J_{12}^2}{Y_P} + Y_P + jJ_{13}}. \tag{17}$$

The $S_{21}$-parameter can then be calculated by

$$S_{21} = \frac{Y_o - Y_e}{(1 + Y_e)(1 + Y_o)}. \tag{18}$$

To study its TZ characteristics, let $S_{21} = 0$, and then, we can obtain

$$Y_P = j\frac{J_{12}^2}{2J_{13}}. \tag{19}$$

This equation indicates that, when $Y_P$ equals a specified imaginary value associated with $J_{12}$ and $J_{13}$, a TZ would be created at the corresponding frequency $\omega_z$. Since $Y_P$ can be represented by (16), we can substitute (16) into (19) and obtain

$$\frac{\omega_z^2 LC - 1}{\omega_z L} = \frac{J_{12}^2}{2J_{13}}. \tag{20}$$

To simplify the derivation, we do not solve this equation but only consider the sign of $J_{13}$. The plus sign of $J_{13}$ means an inductive cross coupling between the nonadjacent resonators, while the minus sign of $J_{13}$ represents a capacitive cross coupling. Therefore, two situations can be considered here.

1) When $J_{13} > 0$, an inductive cross coupling is introduced between the nonadjacent resonators, leading to the right-hand

side of (20) greater than zero. Therefore, to make the left-hand side greater than zero, the following condition should be satisfied:

$$\omega_z^2 LC - 1 > 0, \quad \omega_z > 1/\sqrt{LC} = \omega_0. \tag{21}$$

This formula indicates that a TZ would be created above the passband if an inductive cross coupling is introduced between the first and third resonators.

2) When $J_{13} < 0$, a capacitive cross coupling would be applied, and the right-hand side of (20) would be less than zero. Therefore, the left-hand side should meet the following condition:

$$\omega_z^2 LC - 1 < 0, \quad \omega_z < 1/\sqrt{LC} = \omega_0. \tag{22}$$

This equation suggests that a TZ would be created below the passband if the cross coupling is capacitive.

For the first proposed SIW triplet formed by the meander-line resonator, since an inductive cross coupling is introduced between the two SIW cavities, a TZ would be theoretically generated above the passband. In addition, according to (20), if we change the value of $J_{13}$ with $J_{12}$ fixed, the TZ would be adjustable with variable $J_{13}$.

In order to verify the above theoretical analysis, EM and circuit-based simulations are carried out. The specifications of the triplet are predefined with a center frequency of 10 GHz, an equal-ripple bandwidth of 1.08 GHz, and a TZ placed at 12 GHz. For network circuit synthesis, it can be easily associated with the coupling matrix, and relationships between $J$ inverters and coupling coefficients can be transformed by [48]

$$k_{ij} = \frac{J_{ij}}{\sqrt{b_i b_j}} \tag{23}$$

where $k_{ij}$ represents the coupling coefficients between resonator nodes $i$ and $j$, while $bi$ and $b_j$ are the susceptance slope parameters, which can be obtained by

$$b_i = \frac{\omega_0}{2} \frac{\partial \mathrm{im}(Y_{Pi})}{\omega}\bigg|_{\omega=\omega_0} \tag{24}$$

where $Y_{Pi}$ is the input admittance of the $i$th parallel $LC$ pair.

According to the preset filter specifications, the coupling coefficients and external quality factors can be synthesized as $k_{12} = k_{23} = 0.108$, $k_{13} = 0.036$, and $Q_e = 7.78$.

The filtering responses based on EM simulation and circuit synthesis are presented in Fig. 10, which show good agreement. As expected, a TZ is produced above the passband for the first SIW triplet, presenting consistence with the theoretical analysis. Furthermore, if we tune the cross coupling, namely, change the width of the inductive windows in Fig. 11, the TZ moves closer to the passband with increasing $w_1$. This can be explained from a more intuitive point: When the signal strength of the cross-coupling path increases, in order to cancel it out, the signal strength of the main-coupling path must be also increased; Since signals whose frequencies are close to the passband have higher strength, the TZ would move closer to the passband when the cross coupling increases.

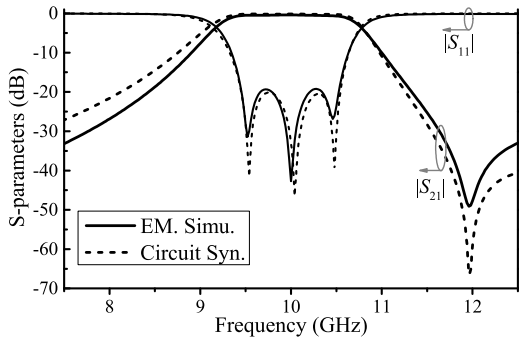


Fig. 10. $S$-parameters of the first triplet based on EM simulation and circuit synthesis.

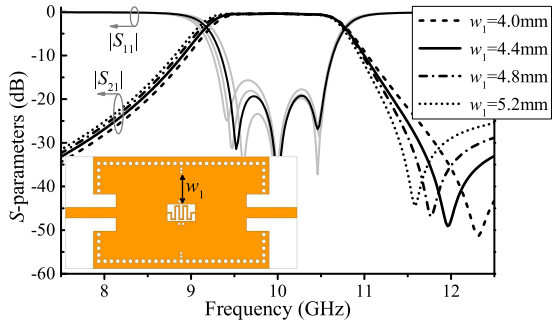


Fig. 11. Simulated $S$-parameters versus variable width ($w_1$) of the coupling window.

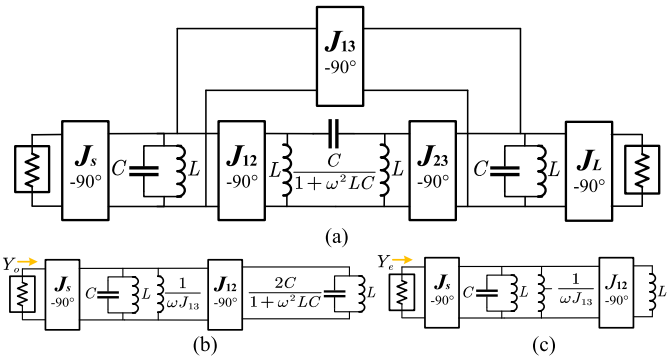


Fig. 12. (a) Network circuit representative of the second SIW triplet. (b) Its odd-mode and (c) even-mode equivalent circuits.

### B. Analysis of the Second SIW Triplet

Fig. 12(a) depicts the equivalent circuit of the second SIW triplet, in which the shunt $LC$ pairs represent the SIW cavities and the $\pi$-type $LC$ circuit represents the CRLH resonator. For conventional network circuit synthesis, all the resonators should be shunt $LC$ pairs, which may not be suited for the proposed circuit with the $\pi$-type resonator. To solve this issue, we can assume that the input admittances of the $\pi$-type and parallel $LC$ circuits are identical. According to (1) and (2), the following equation holds:

$$Y_{\text{in1}} = \frac{1-\omega^2 L_1 C_1}{j\omega L_1} = \frac{1-2\omega^2 L_2 C_2}{j\omega L_2\left(1-\omega^2 L_2 C_2\right)} = Y_{\text{in2}}$$
$$\left(1-\omega^2 L_1 C_1\right)\left(1-\omega^2 L_2 C_2\right) = 1-2\omega^2 L_2 C_2. \tag{25}$$

Assuming that the inductors in the two resonant circuits have the same inductance, namely, $L_1 = L_2$, (25) can be simplified

by replacing $L_2$ with $L_1$, and $C_2$ can be further derived as

$$C_2 = \frac{C_1}{1+\omega^2 L_1 C_1}. \tag{26}$$

This equation indicates that $C_2$ can be represented by a frequency-dependent capacitor associated with $L_1$ and $C_1$. Consequently, in Fig. 12(a), the inductance of the $\pi$-type $LC$ circuit can be considered identical to that of the shunt $LC$ pairs, while the capacitance is expressed as a frequency-dependent value originated from $L$ and $C$.

Considering that the resonant frequency of the parallel $LC$ pairs is calculated by $\omega_0 = 1/\sqrt{LC}$, the resonant frequency of the $\pi$-type circuit can then be represented by (4)

$$\omega_0^{\pi} = \frac{1}{\sqrt{2L\frac{C}{1+\omega^2 LC}}} = \sqrt{\frac{\omega_0^2+\omega^2}{2}}. \tag{27}$$

This formula indicates that, when the frequency variable $\omega$ equals $\omega_0$, the resonant frequency of the $\pi$-type $LC$ circuit would be identical to that of the parallel $LC$ resonators. Although the resonant frequency would change if the frequency variable $\omega$ moves away from $\omega_0$, network circuit synthesis can be considered effective for narrowband responses.

For the circuit shown in Fig. 12(a), its odd- and even-mode equivalent circuits can be extracted as presented in Fig. 12(b) and (c), respectively. The input admittance of the parallel $LC$ pairs can be represented by $Y_P$ in (16).

Therefore, for the odd-mode circuit, its input admittance can be obtained as

$$Y_o = \frac{J_s^2}{\frac{J_{12}^2}{Y_P}\left(1+\omega^2 LC\right) + Y_P - jJ_{13}}. \tag{28}$$

As for the even-mode circuit, its input admittance can be derived as

$$Y_e = \frac{J_s^2}{j\omega L \cdot J_{12}^2 + Y_P + jJ_{13}}. \tag{29}$$

Then, the $S_{21}$-parameter of the equivalent circuit can be calculated by (18). As previously shown, to study the TZ characteristics, let the numerator of the $S_{21}$-parameter vanish, namely, $Y_o$–$Y_e = 0$; then, we can obtain

$$j\omega_z L - \frac{1+\omega_z^2 LC}{Y_P} = -j\frac{2J_{13}}{J_{12}^2}. \tag{30}$$

Note that $Y_P$ can be represented by (16); by substituting it into (30), we obtain

$$\frac{\omega_0^2}{\omega_z^2} \cdot \frac{\omega_z^2 LC - 1}{\omega_z L} = -\frac{J_{12}^2}{J_{13}}. \tag{31}$$

This equation indicates that a TZ would be created at the frequency that makes the left-hand side of the equation equal to the right-hand side. The right-hand side, which is associated with the two $J$ inverters $J_{12}$ and $J_{13}$, determines the position of the TZ. For simplicity, we herein investigate this issue from a more intuitive point instead of solving the equation. Since $J_{13}$ can be an inductive or capacitive cross coupling if it is greater or less than zero, respectively, two situations can be considered.

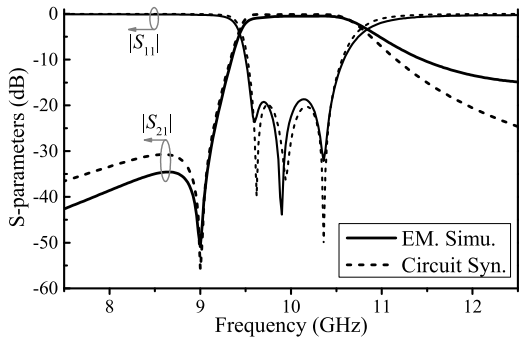


Fig. 13. $S$-parameters of the second triplet based on EM simulation and circuit synthesis.

1) When $J_{13} > 0$, an inductive cross coupling is introduced between the first and third resonators, and the right-hand side of (31) would be less than zero. To make the equation hold, the left-hand side should satisfy the following condition:

$$\omega_z^2 LC - 1 < 0, \quad \omega_z < 1/\sqrt{LC} = \omega_0. \tag{32}$$

This formula indicates that a TZ would be created below the passband if the cross coupling is inductive.

2) When $J_{13} < 0$, the cross coupling is capacitive, and the right-hand side of (31) would be greater than zero. To make the equation hold, the left-hand side should satisfy the following condition:

$$\omega_z^2 LC - 1 > 0, \quad \omega_z > 1/\sqrt{LC} = \omega_0. \tag{33}$$

This formula suggests that a TZ would be created above the passband if the cross coupling is capacitive.

Therefore, for the proposed SIW triplet using a CRLH resonator, a TZ is theoretically generated below the passband because an inductive cross coupling is introduced by the coupling windows. Compared with the meander-line-based triplet, the second triplet presents completely reversed TZ characteristics. Although both triplets have the same sign of the cross couplings introduced by the inductive coupling windows, a TZ would be created above the passband for the triplet using the meander-line resonator, while it is produced below the passband for the triplet employing the CRLH resonator.

To verify the TZ characteristics of the second triplet, EM and circuit-based simulations are performed. The specifications are predefined with a center frequency of 10 GHz, an equal-ripple bandwidth of 0.87 GHz, and a TZ placed at 9 GHz. The synthesized external quality factor and coupling coefficients are $Q_e = 9.86$, $k_{12} = k_{23} = 0.082$, and $k_{13} = 0.033$. Fig. 13 depicts $S$-parameters obtained by EM and circuit-based simulations. As expected, a TZ is generated below the passband, which is consistent with the theoretical results. Furthermore, if we change the strength of the cross coupling, namely, the width of the inductive windows, the TZ is movable and, as shown in Fig. 14, moves closer to the passband with increasing width of the inductive windows. This leads to a controllable TZ that has minor effects on the passband responses.

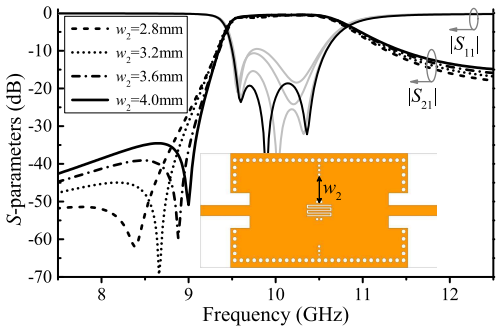


Fig. 14. Simulated $S$-parameters versus variable width ($w_2$) of the coupling window.

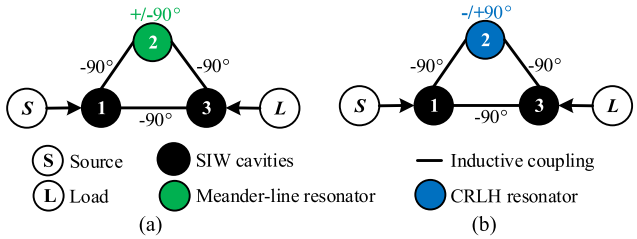


Fig. 15. Signal coupling schemes of (a) first and (b) second SIW triplets.

### C. Mechanism of TZ Generation Using Phase Method

The TZ characteristics of the two SIW triplets have been investigated mathematically in the previous sections. To simplify the derivations, we are using an intuitive approach that utilizes phase analysis [50]. As presented in [50], an inductive coupling would provide a $-90°$ phase shift. For parallel $LC$ resonators, the phase shift is $+90°$ below and $-90°$ above the resonance. Basically, almost all RH resonators, such as SIW cavities, quarter- and half-wavelength microstrip resonators, combline cavity resonators, and rectangular waveguide resonators, fall into this category.

In terms of the proposed two triplets, the SIW cavities can be considered as shunt $LC$ resonators, whose phase shift can be regarded as $+90°$ below and $-90°$ above the resonance. The meander-line and CRLH resonators, as discussed in Section II, present the opposite phase performance. Fig. 15 exhibits the signal coupling schemes of the two triplets, in which the green and blue nodes represent the meander-line and CRLH resonators, respectively. The green node shows a phase shift of $+90°$ below and $-90°$ above the resonance, while the blue node presents a reversed phase shift below and above the resonance.

Tables I and II present phase analyses of the first and second triplets, respectively. For the first triplet, the phase difference through the two coupling paths, namely, the main- and cross-coupling paths, would be in-phase below the passband and out-of-phase above the passband. Therefore, a TZ would be generated above the passband for the first triplet. Reversely, as shown in Table II, the phase difference of the two coupling paths would be out-of-phase below the passband for the second triplet, resulting in a TZ created at the lower band. It also indicates that the two triplets present different TZ performances, which are consistent with the above theoretical analysis.

TABLE I
PHASE ANALYSIS OF THE FIRST TRIPLET

| | $f<f_0^{\mathrm{I}}$ | $f>f_0^{\mathrm{I}}$ |
|---|---|---|
| **Path $R_1^{\mathrm{I}}\rightarrow R_2^{\mathrm{I}}\rightarrow R_3^{\mathrm{I}}$** | -90°+90°-90 = -90° | -90°-90°-90 = -270° |
| **Path $R_1^{\mathrm{I}}\rightarrow R_3^{\mathrm{I}}$** | -90° | -90° |
| **Phase difference** | 0° in-phase | -180° Out-of-phase |
| **Result** | No TZs | A TZ |

TABLE II
PHASE ANALYSIS OF THE SECOND TRIPLET

| | $f<f_0^{\mathrm{II}}$ | $f>f_0^{\mathrm{II}}$ |
|---|---|---|
| **Path $R_1^{\mathrm{II}}\rightarrow R_2^{\mathrm{II}}\rightarrow R_3^{\mathrm{II}}$** | -90°-90°-90 = -270° | -90°+90°-90 = -90° |
| **Path $R_1^{\mathrm{II}}\rightarrow R_3^{\mathrm{II}}$** | -90° | -90° |
| **Phase difference** | -180° Out-of-phase | 0° in-phase |
| **Result** | A TZ | No TZs |

To summarize, conventional resonant nodes (i.e., shunt $LC$ pairs), which present a phase shift of $+90°$ below and $-90°$ above the resonance, are typically used in various filter schematic topologies. These resonant nodes can be quarter- and half-wavelength microstrip resonators, SIW cavities, and combline and/or waveguide resonators in practical applications. In contrast, a CRLH-based resonant node, which presents the reversed phase performance, is proposed to jointly apply in filter coupling topologies for the first time, showing merits in the generation and control of TZs without negative couplings.

### D. Dissipation and Unloaded Quality Factor

It is certain that the microstrip-based meander-line and CRLH resonators cause more energy dissipation than SIW cavities. Basically, the dissipation involves radiation, finite metal conductivity, and dielectric loss of the substrate. To study how these factors affect the loss of the two SIW triplets, Fig. 16 presents the simulated radiation, metal, and substrate loss rates. As seen, the metal loss is more dominant than other losses, and meander-line and CRLH resonators cause higher metal losses at the corresponding resonant frequencies than that of the SIW cavities. This is simply explained that larger current densities are produced in the meander-line and CRLH resonators due to their small size, which, thereby, causes more resistive dissipation. In addition, for the meander-line resonator, its radiation and substrate losses are at a low level, which is almost identical to that of the SIW cavities, while, for the CRLH resonator, its radiation and substrate losses minorly rise at the corresponding frequency comparing to that caused by the SIW cavities. Overall, the metal loss is the dominant factor that leads to increased dissipation although a small amount of radiation and substrate losses can also be produced by the CRLH resonator.

According to [51], the relationship between dissipation and unloaded quality factor is associated with insertion loss (IL) $A_0$ at the band center, which is evaluated as

$$A_0 \approx 20 \log e \cdot \delta \cdot \tau_0 \tag{34}$$

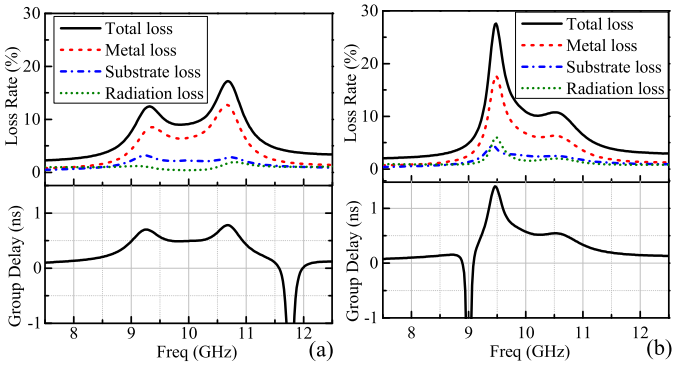


Fig. 16. Simulated loss rates and group delays of (a) meander-line-based SIW triplet and (b) CRLH-based SIW triplet.

where $\delta$ is the dissipation factor, which can be represented by $\delta = 1/(FBW \cdot Q_u)$. $\tau_0$ is the absolute group delay at $\omega = 0$ of the low-pass prototype, and its relationship in a bandpass filter can be transformed by $\tau_0 \approx (\Delta\omega \cdot \tau_{\mathrm{BPF}})/2$. Therefore, the average unloaded quality factors of the SIW triplets can be calculated if their ILs and group delays are given.

As depicted in Fig. 16(a) and (b), the simulated group delays are 0.494 and 0.572 ns for the two triplets, while the simulated ILs are 0.396 and 0.528 dB, respectively. According to (34), the calculated average unloaded quality factor is $Q_u^I = 340.6$ for the first triplet and $Q_u^{II} = 272.8$ for the second triplet. These calculated average $Q_u$ values are greater than that of the individual meander-line and CRLH resonators shown in Fig. 2. Compared with the SIW cavity whose $Q_u$ is around 434 by eigenmode simulation, the two SIW triplets present moderate quality factors between SIW and microstrip resonators.

## IV. Triplet Filters With Quasi-Elliptic Responses

Using the reversed TZ characteristics of the two triplets, their application to quasi-elliptic filters is investigated in this section. Two quasi-elliptic filters, which are realized by parallel and cascaded triplet topologies, are designed to present four- and five-pole responses with a TZ created at both sides of the passbands.

### A. Parallel Triplet Quasi-Elliptic Filter

Fig. 17(a) shows the configuration of the proposed parallel triplet filter, which is also known as the transversal filter. The meander-line and CRLH resonators are etched between the two SIW cavities, constituting two parallelly arranged triplets. The metallic-via arrays, which are placed around the meander-line and CRLH resonators, are used to tune the couplings between the microstrip and SIW resonators. An inductive coupling window with a width of $w_c$ is constructed to adjust the cross coupling. With such a filter configuration, its coupling topology can be depicted, as shown in Fig. 17(b), in which the green and blue resonant nodes represent the meander-line and CRLH resonators, respectively. In addition, it is also worth noting that all the couplings between the resonators are inductive.

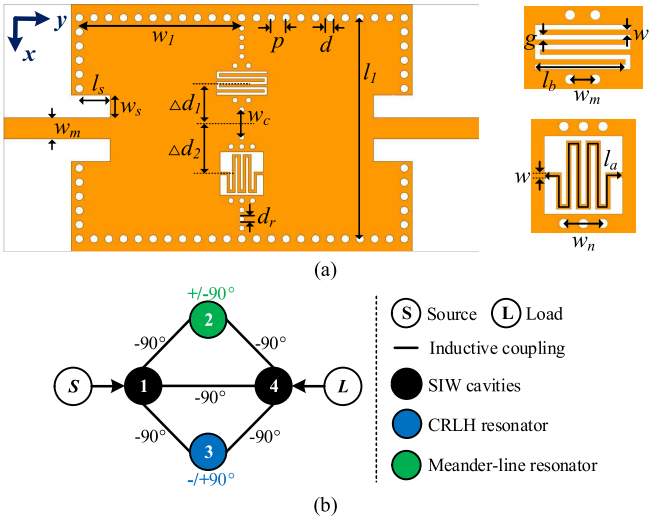


Fig. 17. (a) Layout of the parallel triplet quasi-elliptic filter. (b) Its coupling schematic topology. (Initial dimensions in mm: $l_1 = 16.6$, $w_1 = 12.1$, $l_s = 2.3$, $w_s = 1.7$, $w_m = 1.57$, $\Delta d_1 = 3.4$, $\Delta d_2 = 3.4$, $w_c = 2.1$, $d_r = 0.4$, $d = 0.6$, $p < 1$, $l_a = 16.45$, $l_b = 3.57$, $w = 0.2$, $w_m = 1$, $w_n = 1.6$, and $g = 0.2$.)

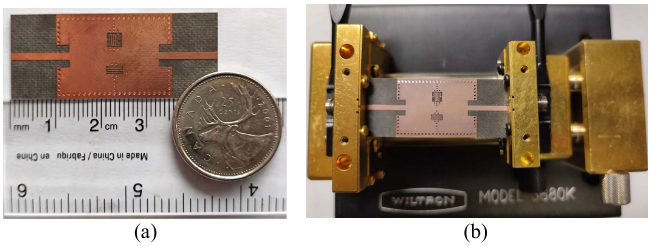


Fig. 18. (a) Photograph of the fabricated parallel triplet quasi-elliptic filter. (b) Photograph of the measurement setup with an Anritsu 3680 test fixture.

To illustrate the design process, the synthesis of a quasi-elliptic filter operating in the $X$-band is performed. The specifications of the filter are predefined as follows.

1) *Center Frequency:* 10 GHz.
2) *In-Band Return Loss:* 20 dB.
3) *Equal-Ripple Bandwidth:* 1 GHz ($\Delta = 10\%$).
4) *TZs:* 8.7 and 11.62 GHz.

According to the specifications, the synthesized external quality factor and coupling coefficients can be extracted by the circuit synthesis procedure as $Q_e = 9.36$, $k_{12} = k_{24} = 0.0657$, $k_{13} = k_{34} = 0.0626$, and $k_{14} = 0.0036$.

These parameters can be considered as design guidelines for the filter, which can determine its initial dimensions. For demonstration, a filter prototype is designed and fabricated on Rogers RT/Duriod 5880 substrate with a relative dielectric constant of 2.2, a thickness of 0.508 mm, and a loss tangent of 0.0009. Fig. 18 shows the photograph of the fabricated filter, whose circuit size is $16.6 \times 24.2$ mm$^2$ ($0.60\lambda_g \times 0.88\lambda_g$). To better present the filter performance, a thru-reflect-line (TRL) calibration was used to obtain the experimental results.

Fig. 19 presents the circuit-synthesized, EM-simulated, and measured $S$-parameters and group delays, which are in good agreement. The measured center frequency is 10.05 GHz with a 3-dB bandwidth of 1.23 GHz, while the simulated values

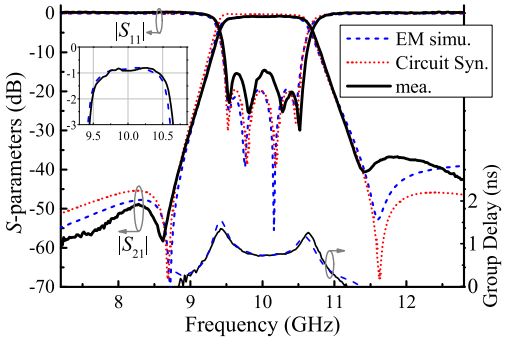


Fig. 19. Circuit-synthesized, EM-simulated, and measured $S$-parameters and group delay of the parallel triplet filter.

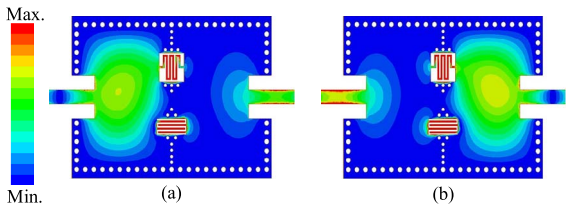


Fig. 20. Passband electric field distributions of the first triplet filter at (a) $t = 0$ and (b) $t = T/4$.

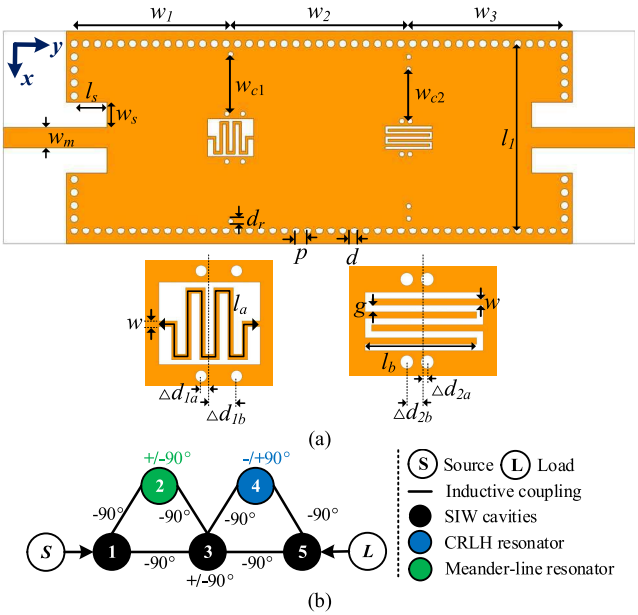


Fig. 21. (a) Layout of the cascaded triplet quasi-elliptic filter. (b) Its coupling topology. (Initial dimensions in mm: $l_1 = 14.8$, $w_1 = 12.35$, $w_2 = 14.06$, $w_3 = 12.3$, $l_s = 2.6$, $w_s = 2$, $w_m = 1.57$, $w_{c1} = 4.7$, $w_{c2} = 4.1$, $d_r = 0.4$, $d = 0.6$, $p < 1$, $l_a = 15.44$, $l_b = 3.48$, $w = 0.2$, $g = 0.2$, $\Delta d_{1a} = 0.3$, $\Delta d_{1b} = 0.96$, $\Delta d_{2a} = 0.1$, and $\Delta d_{2b} = 0.54$.)

are 10 GHz and a 3-dB bandwidth of 1.19 GHz. The slightly shifted passband is attributed to fabrication tolerances, which moves the passband center to a higher frequency. In addition, the measured return loss is greater than 14.5 dB with a minimal IL of 0.82 dB, which is almost identical to the simulated IL of 0.8 dB. As observed, the proposed filter presents a quasi-elliptic response with a TZ located at both sides of the passband, showing a high selectivity. To calculate the average quality factor of the filter, the simulated IL and group delay at the band center are 0.84 dB and 0.726 ns. According to (34), the calculated average $Q_u$ is 235.8.

Fig. 20 exhibits the electric field distributions of the proposed filter at $t = 0$ and $t = T/4$, where $T$ is the period of the signal. The value $t = 0$ represents the initial time (an initial phase is selected which may not be 0°) when the SIW cavity is excited, and $t = T/4$ depicts the varied electric distributions after a quarter period. The two SIW cavities operate in the $TE_{101}$ mode, while the meander-line and CRLH resonators resonate at their dominant modes. These two microstrip resonators are excited simultaneously in this parallel filter topology. The mode transformation between the microstrip and SIW resonators is observed, which produces a signal transmission path.

### B. Cascaded Triplet Quasi-Elliptic Filter

Fig. 21(a) shows the second quasi-elliptic filter based on the cascaded triplet configuration. The meander-line and CRLH resonators are each etched between two SIW cavities, creating two triplet sections. Noting that the second SIW cavity is shared by the two triplets, resulting in the cascaded topology. In addition, as shown in Fig. 21(a), asymmetric metallic-via arrays are placed around the meander-line and CRLH resonators to adjust the couplings between each microstrip resonator and the adjacent SIW cavities. Similar to the first filter, symmetric coupling windows are constructed between every two SIW cavities to produce cross couplings for each triplet. With such a filter configuration, its coupling topology can be depicted, as shown in Fig. 21(b), in which all couplings are inductive. Two triplet loops, which includes green and blue resonant nodes, share the mutual resonant node 3 in this cascaded topology. As discussed before, a TZ is created above the passband by the triangular loop with the blue node, while the other TZ is created below the passband in the green triangular loop.

To demonstrate the proposed concept, a filter prototype operating in the $X$-band is synthesized with a fifth-order quasi-elliptic response. The specifications are predefined as follows.

1) *Center Frequency:* 10 GHz.
2) *In-Band Return Loss:* 20 dB.
3) *Equal-Ripple Bandwidth:* 1.16 GHz ($\Delta = 11.6\%$).
4) *TZs:* 8.84 and 12.16 GHz.

According to the specifications, the synthesized parameters can be obtained by a circuit optimization procedure as $Q_e = 8.32$, $k_{12} = 0.0974$, $k_{23} = 0.0714$, $k_{34} = 0.067$, $k_{45} = 0.0959$, $k_{13} = 0.0191$, and $k_{35} = 0.0274$, where $Q_e$ and $k_{ij}$ represent the external quality factor and coupling coefficients, respectively.

For validation, a filter design is performed using a fine synthesis and optimization process, and the prototype is fabricated on the Rogers RT/Duriod 5880 substrate. Fig. 22 shows a photograph of the manufactured filter, whose circuit size is $14.8 \times 38.71$ mm$^2$ ($0.49\lambda_g \times 1.27\lambda_g$). A TRL calibration was applied for the measurement.

The measured $S$-parameters and group delays, together with the EM-simulation and circuit-synthesis results, are presented

TABLE III
COMPARISON WITH OTHER REPORTED CROSS-COUPLED FILTERS

| | Technology | Resonant nodes | $f_0$ (GHz)/3-dB FBW | IL (dB) | $Q_u$ | Order | Number of TZs | TZ Control | The need of negative couplings | Circuit Size ($\lambda_g \times \lambda_g$) |
|---|---|---|---|---|---|---|---|---|---|---|
| [31] | Combline cavity | 6 shunt *LC* pairs | 1.54/ 3.1% | < 1dB | 4900 | 6 | 2 | Y | Y (capacitive probe) | N/A |
| [32] | SIW | 4 hunt *LC* pairs | 20.5 / 3.9% | 0.9 | 500 | 4 | 2 | Y | Y (S-shape slots) | 0.93×0.97 |
| | | | | 1.0 | 500 | 4 | 4 | Y | Y (S-shape slots) | 1.22×0.97 |
| [33] | Coaxial SIW | 4 shunt *LC* pairs | 5.75 / 2.0% | 3.6 | 225 | 4 | 2 | Y | Y (CPW line) | 0.86 × 0.86 |
| [34] | SIW | 4 Shunt *LC* pairs | 5.5 / 12.1% | 1.68 | N/A | 4 | 2 | Y | Y (H-shape slot) | 1.07 × 1.11 |
| | | | 5.8 / 2.51% | 6.35 | N/A | 4 | 2 | Y | Y (H-shape slot) | 1.26 × 1.25 |
| [35] | QMSIW | 4 Shunt *LC* pairs | 5 / 11.3 | 1.85 | 150 | 4 | 2 | Y | Y (interdigital unit) | 0.73×0.71 |
| [36] | Multilayer SIW | 4 Shunt *LC* pairs | 12.75 / 4.2% | 3.0 | N/A | 4 | 2 | Y | Y (circular aperture) | N/A |
| | | | 12.65 / 4.0% | 3.0 | N/A | 4 | 2 | Y | Y (circular aperture) | N/A |
| [37] | Multilayer SIW | 4 Shunt *LC* pairs | 20.1 / 2.5% | 2.6 | N/A | 4 | 2 | Y | Y (V-shape unit) | N/A |
| **This Work** | SIW & microstrip | 1 π-type node and 3 shunt *LC* pairs | 10.05 / 12.2% | 0.82 | 235.8 | 4 | 2 | Y | N | 0.60×0.88 |
| | | 1 π-type node and 4 shunt *LC* pairs | 10.14 / 12.9% | 0.91 | 292.2 | 5 | 2 | Y | N | 0.49×1.27 |

N/A: Not Applicable;

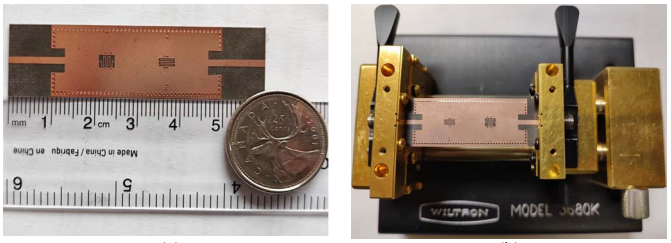


(a) (b)

Fig. 22. (a) Photograph of the fabricated cascaded triplet quasi-elliptic filter. (b) Photograph of the measurement setup with an Anritsu 3680 test fixture.

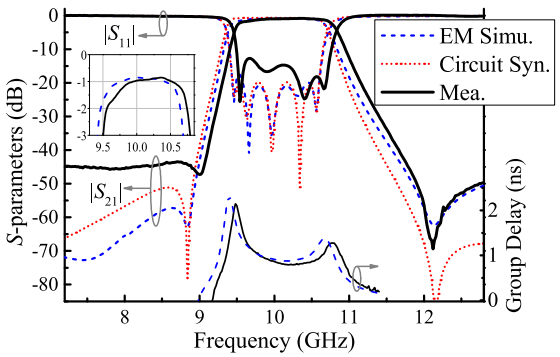


Fig. 23. Circuit-synthesized, EM-simulated, and measured *S*-parameters and group delay of the cascaded triplet quasi-elliptic filter.

in Fig. 23, which shows quasi-elliptic responses with good agreement. The measured center frequency is 10.14 GHz compared with the simulation of 10 GHz. The measured 3-dB bandwidth is 1.31 GHz with a minimal IL of 0.91 dB, while it is 1.27 GHz with a minimal IL of 0.85 dB in the simulation. The measured return loss is greater than 12.7 dB within the passband. As is expected, the filter presents a high selectivity with TZs created at both sides of the passband. Although the measured passband slightly moves up in frequency due to the fabrication tolerance, the measured *S*-parameters present an excellent electrical performance with low loss and high selectivity. Since the simulated IL and group delay at the band

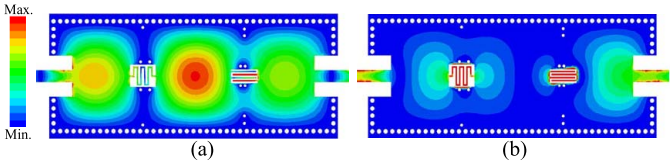


(a) (b)

Fig. 24. Passband electric field distributions of the second triplet filter at (a) $t = 0$ and (b) $t = T/4$.

center are 0.849 dB and 0.909 ns, the average $Q_u$ is calculated as 292.2. In addition, the measured out-of-band rejection declines below the passband compared to the simulation, which is caused by an unexpected mode weakly excited at the lower band. The shifted first TZ also contributes to the degraded rejection level.

Fig. 24 shows the passband electric field distributions of the filter at $t = 0$ and $t = T/4$. The mode transformation between the $TE_{101}$ mode and the dominant modes of the microstrip resonators is observed during the transmission of signals, which generates the coupling path of the passband.

## V. COMPARISONS AND DISCUSSION

To demonstrate the advantages of the proposed filters, a performance comparison with other reported cross-coupled filters is presented in Table III. For conventional waveguide filters, such as combline and SIW filters, all resonant nodes can be considered as typical shunt *LC* pairs, and inductive couplings are easily achieved by coupling windows. However, in order to achieve quasi-elliptic filtering responses, electric cross-coupling structures, such as a capacitive probe in [31], S-shape slots in [32], a CPW line in [33], an H-shape slot in [34], an interdigital unit in [35], a circular aperture in [36], and a V-shape unit are indispensable to introduce negative couplings. On the contrary, a CRLH resonant node, which is equivalent to a $\pi$-type *LC* circuit, is applied in the proposed filters. Due to its reversed phase shift characteristics compared with shunt *LC* resonant nodes, an inductive cross coupling can be used to create a TZ below the passband, which, thereby, eliminates the need for negative couplings. As is well

known, it is quite simple and convenient to achieve inductive couplings in waveguide filters, while electric-cross structures would introduce some radiation loss and increase design complexity on the SIW platform. Therefore, the proposed filters show advantages to achieve quasi-elliptic responses with all inductive couplings. In addition, they also show other outstanding electrical performances, such as low loss and compactness. Compared with the fourth-order full-mode SIW filters in [32] and [34], the proposed filters show significant size reduction with moderate $Q_u$. As to the fourth-order quasi-elliptic QMSIW filter in [35], our first filter almost exhibits comparable circuit size but has higher $Q_u$.

## VI. Conclusion

In this article, a comprehensive investigation into the meander-line and CRLH resonators and their applications to quasi-elliptic SIW-based filters is presented. The resonance and transfer characteristics of the two resonators are well studied by theoretical derivations and simulation. The meander-line resonator can be considered a typical RH resonator, which is generally equivalent to a parallel *LC* resonant pair, while, for the CRLH resonator, a series capacitance would be dominant. Due to these variations, the two resonators present completely opposite phase shift responses below and above their resonant frequencies. By utilizing this feature, two SIW triplets, including meander-line and CRLH resonators, are proposed, which are able to generate a TZ each above and below the passband if an inductive cross coupling exists. This feature shows the merit that TZs can be generated without using negative couplings. For demonstration, two filter prototypes realized by parallel and cascaded triplet topologies are designed, prototyped, and measured and achieve quasi-elliptic responses with good electrical performance, including compactness, low loss, and high selectivity.

In conclusion, this article presents a new technique combining conventional resonant nodes with a CRLH node in SIW filter design. Different from using purely conventional resonant nodes (i.e., shunt *LC* pairs) or CRLH nodes, a joint application of these two types of resonant nodes is developed for the first time, which shows the merit of introducing TZs at both sides of the passband without the need for negative couplings. The proposed technique can be considered a feasible way in advanced filter design, especially for quasi-elliptic filter applications with high selectivity and low loss in satellite and mobile communications. It can also be extended to other types of filters such as waveguide and combline filters, especially in scenarios where negative couplings are not easy to achieve and miniaturization is required.

## References


[1] G. Moloudian, S. Bahrami, and R. M. Hashmi, "A microstrip lowpass filter with wide tuning range and sharp roll-off response," *IEEE Trans. Circuits Syst. II, Exp. Briefs*, vol. 67, no. 12, pp. 2953–2957, Dec. 2020.

[2] E. Arabi, M. Lahti, T. Vaha-Heikkila, and A. Shamim, "A 3-D miniaturized high selectivity bandpass filter in LTCC technology," *IEEE Microw. Wireless Compon. Lett.*, vol. 24, no. 1, pp. 8–10, Jan. 2014.

[3] G. Macchiarella, "Synthesis of an in-line prototype filter with two transmission zeros without cross couplings," *IEEE Microw. Wireless Compon. Lett.*, vol. 14, no. 1, pp. 19–21, Jan. 2004.

[4] S. Amari and U. Rosenberg, "Synthesis and design of novel in-line filters with one or two real transmission zeros," *IEEE Trans. Microw. Theory Techn.*, vol. 52, no. 5, pp. 1464–1478, May 2004.

[5] S. Amari and G. Macchiarella, "Synthesis of inline filters with arbitrarily placed attenuation poles by using nonresonating nodes," *IEEE Trans. Microw. Theory Techn.*, vol. 53, no. 10, pp. 3075–3081, Oct. 2005.

[6] G. Macchiarella, "Generalized coupling coefficient for filters with non-resonant nodes," *IEEE Microw. Wireless Compon. Lett.*, vol. 18, no. 12, pp. 773–775, Dec. 2008.

[7] O. Glubokov and D. Budimir, "Extraction of generalized coupling coefficients for inline extracted pole filters with nonresonating nodes," *IEEE Trans. Microw. Theory Techn.*, vol. 59, no. 12, pp. 3023–3029, Dec. 2011.

[8] Y. Yang, M. Yu, and Q. Wu, "Advanced synthesis technique for unified extracted pole filters," *IEEE Trans. Microw. Theory Techn.*, vol. 64, no. 12, pp. 4463–4472, Dec. 2016.

[9] E. Guerrero, J. Verdu, and P. de Paco, "Synthesis of extracted pole filters with transmission zeros in both stopbands and nonresonant nodes of the same nature," *IEEE Microw. Wireless Compon. Lett.*, vol. 31, no. 1, pp. 17–20, Jan. 2021.

[10] J. Verdu, E. Guerrero, L. Acosta, and P. de Paco, "Exact synthesis of inline fully canonical dual-band filters using dual extracted-pole sections," *IEEE Microw. Wireless Compon. Lett.*, vol. 31, no. 12, pp. 1255–1258, Dec. 2021.

[11] Q.-X. Chu and H. Wang, "A compact open-loop filter with mixed electric and magnetic coupling," *IEEE Trans. Microw. Theory Techn.*, vol. 56, no. 2, pp. 431–439, Feb. 2008.

[12] Q. Liu, D. Zhang, D.-F. Zhou, Y. Liu, and D. Lv, "Inline asymmetric response quarter-mode SIW bandpass filters with controllable mixed electric and magnetic coupling," in *Proc. Int. Symp. Antennas Propag. (ISAP)*, Xi'an, China, 2019, pp. 1–3.

[13] L. Szydlowski, A. Jedrzejewski, and M. Mrozowski, "A trisection filter design with negative slope of frequency-dependent crosscoupling implemented in substrate integrated waveguide (SIW)," *IEEE Microw. Wireless Compon. Lett.*, vol. 23, no. 9, pp. 456–458, Sep. 2013.

[14] S. Tamiazzo and G. Macchiarella, "Synthesis of cross-coupled filters with frequency-dependent couplings," *IEEE Trans. Microw. Theory Techn.*, vol. 65, no. 3, pp. 775–782, Mar. 2017.

[15] P. Zhao and K. Wu, "Cascading fundamental building blocks with frequency-dependent couplings in microwave filters," *IEEE Trans. Microw. Theory Techn.*, vol. 67, no. 4, pp. 1432–1440, Apr. 2019.

[16] S. Zhang, L. Zhu, and R. Weerasekera, "Synthesis of inline mixed coupled quasi-elliptic bandpass filters based on $\lambda/4$ resonators," *IEEE Trans. Microw. Theory Techn.*, vol. 63, no. 10, pp. 3487–3493, Oct. 2015.

[17] S. Amari and U. Rosenberg, "Characteristics of cross (bypass) coupling through higher/lower order modes and their applications in elliptic filter design," *IEEE Trans. Microw. Theory Techn.*, vol. 53, no. 10, pp. 3135–3141, Oct. 2005.

[18] F. Zhu, W. Hong, J.-X. Chen, and K. Wu, "Cross-coupled substrate integrated waveguide filters with improved stopband performance," *IEEE Microw. Wireless Compon. Lett.*, vol. 22, no. 12, pp. 633–635, Dec. 2012.

[19] M. Salehi, J. Bornemann, and E. Mehrshahi, "Compact folded substrate integrated waveguide filter with non-resonating nodes for high-selectivity bandpass applications," in *Proc. 43rd Eur. Microw. Conf.*, Nuremberg, Germany, Oct. 2013, pp. 155–158.

[20] D. Miek, P. Boe, F. Kamrath, and M. Höft, "Techniques for the generation of multiple additional transmission zeros in H-plane waveguide filters," *Int. J. Microw. Wireless Technol.*, vol. 12, no. 8, pp. 723–732, Oct. 2020.

[21] Q. Liu, D. Zhou, D. Zhang, and D. Lv, "SIW bandpass filters in modified box-section scheme with bypass/constant/frequency-dependent coupling in diagonal cross-coupling path," *IET Microw., Antennas Propag.*, vol. 13, no. 5, pp. 559–566, Apr. 2019.

[22] J.-Q. Ding, S.-C. Shi, K. Zhou, Y. Zhao, D. Liu, and W. Wu, "WR-3 band quasi-elliptical waveguide filters using higher order mode resonances," *IEEE Trans. THz Sci. Technol.*, vol. 7, no. 3, pp. 302–309, May 2017.

[23] Y.-W. Wu, Z.-C. Hao, R. Lu, and J.-S. Hong, "A high-selectivity D-band mixed-mode filter based on the coupled overmode cavities," *IEEE Trans. Microw. Theory Techn.*, vol. 68, no. 6, pp. 2331–2342, Jun. 2020.

[24] R. J. Cameron, "Advanced coupling matrix synthesis techniques for microwave filters," *IEEE Trans. Microw. Theory Techn.*, vol. 51, no. 1, pp. 1–10, Jan. 2003.

[25] U. Rosenberg, M. Knipp, and S. Amari, "Compact diplexer design using different E-plane triplets to serve contiguous passbands with high interband selectivity," in *Proc. Eur. Microw. Conf.*, Manchester, U.K., Sep. 2006, pp. 133–136.
[26] S. Sirci, J. D. Martinez, J. Vague, and V. E. Boria, "Substrate integrated waveguide diplexer based on circular triplet combline filters," *IEEE Microw. Wireless Compon. Lett.*, vol. 25, no. 7, pp. 430–432, Jul. 2015.
[27] J.-S. Hong and M. J. Lancaster, "Couplings of microstrip square open-loop resonators for cross-coupled planar microwave filters," *IEEE Trans. Microw. Theory Techn.*, vol. 44, no. 11, pp. 2099–2109, Nov. 1996.
[28] J.-Q. Ding, S.-C. Shi, K. Zhou, D. Liu, and W. Wu, "Analysis of 220-GHz low-loss quasi-elliptic waveguide bandpass filter," *IEEE Microw. Wireless Compon. Lett.*, vol. 27, no. 7, pp. 648–650, Jul. 2017.
[29] M. Yuceer, "A reconfigurable microwave combline filter," *IEEE Trans. Circuits Syst. II, Exp. Briefs*, vol. 63, no. 1, pp. 84–88, Jan. 2016.
[30] R. Tkadlec and G. Macchiarella, "Pseudoelliptic combline filter in a circularly shaped tube," in *IEEE MTT-S Int. Microw. Symp. Dig.*, Philadelphia, PA, USA, Jun. 2018, pp. 1099–1102.
[31] Y. Wang and M. Yu, "True inline cross-coupled coaxial cavity filters," *IEEE Trans. Microw. Theory Techn.*, vol. 57, no. 12, pp. 2958–2965, Dec. 2009.
[32] X.-P. Cheng and K. Wu, "Substrate integrated waveguide cross-coupled filter with negative coupling structure," *IEEE Trans. Microw. Theory Techn.*, vol. 56, no. 1, pp. 142–149, Jan. 2008.
[33] S. Sirci, F. Gentili, J. D. Martinez, V. E. Boria, and R. Sorrentino, "Quasi-elliptic filter based on SIW combline resonators using a coplanar line cross-coupling," in *IEEE MTT-S Int. Microw. Symp. Dig.*, Phoenix, AZ, USA, May 2015, pp. 1–4.
[34] C. J. You, Z. N. Chen, X. W. Zhu, and K. Gong, "Single-layered SIW post-loaded electric coupling-enhanced structure and its filter applications," *IEEE Trans. Microw. Theory Techn.*, vol. 61, no. 1, pp. 125–130, Jan. 2013.
[35] Y. Shi, K. Zhou, C. Zhou, and W. Wu, "Compact QMSIW quasi-elliptic filter based on a novel electric coupling structure," *Electron. Lett.*, vol. 53, no. 23, pp. 1528–1530, Nov. 2017.
[36] F. Yang and H.-X. Yu, "Two novel substrate integrated waveguide filters in LTCC technology," in *Proc. Int. Conf. Microw. Millim. Wave Technol.*, Chengdu, China, May 2010, pp. 229–232.
[37] B. Lee, S. Nam, C. Kwak, and J. Lee, "New negative coupling structure for $K$-band substrate-integrated waveguide resonator filter with a pair of transmission zeros," *IEEE Microw. Wireless Compon. Lett.*, vol. 28, no. 2, pp. 135–137, Feb. 2018.
[38] T. Martin, A. Ghiotto, T.-P. Vuong, K. Wu, and F. Lotz, "Compact quasi-elliptic and highly selective AFSIW filter with multilayer cross-coupling," in *IEEE MTT-S Int. Microw. Symp. Dig.*, Boston, MA, USA, Jun. 2019, pp. 718–721.
[39] L. Zhou, Z. Long, H. Li, T. Zhang, and M. Qiao, "A novel configuration for compact HTS CQ structure linear phase filter design," *IEEE Trans. Appl. Supercond.*, vol. 28, no. 8, pp. 1–8, Oct. 2018.
[40] N. Sekiya and S. Sugiyama, "Design of miniaturized HTS dual-band bandpass filters using stub-loaded meander line resonators and their applications to tri-band bandpass filters," *IEEE Trans. Appl. Supercond.*, vol. 25, no. 3, pp. 1–5, Jun. 2015.
[41] Z. Ying et al., "A compact superconducting bandpass filter at 360 MHz with very wide stopband using modified spiral resonators," *IEEE Trans. Appl. Supercond.*, vol. 23, no. 1, Feb. 2013, Art. no. 1500706.
[42] T. Yang, M. R. M. Hashemi, P.-L. Chi, and T. Itoh, "A new way of bandpass filter design based on zeroth-order and negative-order resonance modes," in *Proc. Asia Pacific Microw. Conf.*, Singapore, Dec. 2009, pp. 163–166.
[43] N. Amani and A. Jafargholi, "Zeroth-order and $TM_{10}$ modes in one-unit cell CRLH mushroom resonator," *IEEE Antennas Wireless Propag. Lett.*, vol. 14, pp. 1396–1399, 2015.
[44] Q. Cai, W. Che, G. Shen, and Q. Xue, "Wideband high-efficiency power amplifier using D/CRLH bandpass filtering matching topology," *IEEE Trans. Microw. Theory Techn.*, vol. 67, no. 6, pp. 2393–2405, Jun. 2019.
[45] Q.-L. Zhang, B.-Z. Wang, D.-S. Zhao, and K. Wu, "A compact half-mode substrate integrated waveguide bandpass filter with wide out-of-band rejection," *IEEE Microw. Compon. Lett.*, vol. 26, no. 7, pp. 501–503, Jul. 2016.
[46] G. Lin and Y. Dong, "A compact, hybrid SIW filter with controllable transmission zeros and high selectivity," *IEEE Trans. Circuits Syst. II, Exp. Briefs*, vol. 69, no. 4, pp. 2051–2055, Apr. 2022, doi: 10.1109/TCSII.2022.3144268.
[47] J. Tang, H. Liu, and Y. Yang, "Balanced dual-band superconducting filter using stepped-impedance resonators with high band-to-band isolation and wide stopband," *IEEE Trans. Circuits Syst. II, Exp. Briefs*, vol. 68, no. 1, pp. 131–135, Jan. 2021.
[48] J. S. Hong and M. J. Lancaster, *Microstrip Filters for RF/Microwave Applications*. New York, NY, USA: Wiley, 2001.
[49] C. Caloz and T. Itoh, *Electromagnetic Metamaterials: Transmission Line Theory and Microwave Applications*. New York, NY, USA: Wiley, 2005.
[50] J. B. Thomas, "Cross-coupling in coaxial cavity filters—A tutorial overview," *IEEE Trans. Microw. Theory Techn.*, vol. 51, no. 4, pp. 1368–1376, Apr. 2003.
[51] R. J. Cameron, C. M. Kudsia, and R. R. Mansour, *Microwave Filters for Communication Systems: Fundamentals, Design, and Applications*. Hoboken, NJ, USA: Wiley, 2018.

**Yilong Zhu** (Member, IEEE) was born in Chengdu, Sichuan, China, in 1992. He received the B.E. degree in information display and optoelectronic technology from the University of Electronic Science and Technology of China (UESTC), Chengdu, in 2015, and the M.S. degree in circuits and systems from Beihang University, Beijing, China, in 2018. He is currently pursuing the Ph.D. degree in electromagnetic field and microwave techniques at UESTC.

He has been a Visiting Ph.D. Student with the Department of Electrical and Computer Engineering, University of Victoria, Victoria, BC, Canada, since 2021. His research interests include the synthesis design of planar microwave and millimeter-wave filters/diplexers, and surface acoustic wave (SAW) filters for mobile communication.

**Yuandan Dong** (Senior Member, IEEE) received the B.S. and M.S. degrees from the Department of Radio Engineering, Southeast University, Nanjing, China, in 2006 and 2008, respectively, and the Ph.D. degree from the Department of Electrical Engineering, University of California at Los Angeles (UCLA), Los Angeles, CA, USA, in 2012.

From 2008 to 2012, he was a Graduate Student Researcher with the Microwave Electronics Laboratory, UCLA. From 2012 to 2016, he was a Senior Engineer with the Research and Development Hardware Department, Qualcomm, San Diego, CA, USA. From 2016 to 2017, he was a Staff Engineer with Universal Electronics Inc., Santa Ana, CA, USA. Since 2017, he has been a Full Professor with the University of Electronic Science and Technology of China (UESTC), Chengdu, China. He has authored or coauthored more than 230 journal articles and conference papers, which received more than 4900 citations. He holds more than 80 patents, including six international patents. He and his team have developed multiple RF products, including acoustic wave filters, antenna tuners, and antennas, which are very widely shipped and applied in mobile devices. His research interests include the characterization and development of RF and microwave components, RF modules, circuits, antennas, acoustic-wave filters, and metamaterials.

Dr. Dong is a technical program committee member of several international conferences. He was a recipient of the Best Student Paper Award from the 2010 IEEE Asia Pacific Microwave Conference (APMC), Yokohama, Japan, the Best Paper Award in the 2021 IEEE International Wireless Symposium (IWS), the Distinguished Expert Presented by Sichuan Province and the China Government, and the High Level Innovative and Entrepreneurial Talent presented by Jiangsu Province. He is serving as an Associate Editor for the IEEE TRANSACTIONS ON ANTENNAS AND PROPAGATION and the IEEE OPEN JOURNAL OF ANTENNAS AND PROPAGATION. He is serving as a Reviewer for multiple IEEE and IET journals, including the IEEE TRANSACTIONS ON MICROWAVE THEORY AND TECHNIQUES and the IEEE TRANSACTIONS ON ANTENNAS AND PROPAGATION.

**Jens Bornemann** (Life Fellow, IEEE) received the Dipl.Ing. and Dr.Ing. degrees in electrical engineering from the University of Bremen, Bremen, Germany, in 1980 and 1984, respectively.

From 1984 to 1985, he worked as an engineering consultant. In 1985, he joined the University of Bremen as an Assistant Professor. Since April 1988, he has been with the Department of Electrical and Computer Engineering, University of Victoria, Victoria, BC, Canada, where he became a Professor in 1992. From 1992 to 1995, he was a Fellow with the British Columbia Advanced Systems Institute, Vancouver, BC, Canada. In 1996, he was a Visiting Scientist with Spar Aerospace Ltd., (currently MDA Space), Sainte-Anne-de-Bellevue, QC, Canada, and a Visiting Professor with the Microwave Department, Ulm University, Ulm, Germany. From 1997 to 2002, he was the Co-Director of the Center for Advanced Materials and Related Technology, University of Victoria. In 2003, he was a Visiting Professor with the Laboratory for Electromagnetic Fields and Microwave Electronics, ETH Zürich, Zürich, Switzerland. He has coauthored *Waveguide Components for Antenna Feed Systems: Theory and Design* (Artech House, 1993) and has authored/coauthored more than 350 technical papers. His research activities include RF/wireless/microwave/millimeter-wave components, systems and antenna design, and field-theory-based modeling of integrated circuits, feed networks, and antennas.

Dr. Bornemann is a Fellow of the Canadian Academy of Engineering and the Engineering Institute of Canada and serves on the Editorial Advisory Board of the *International Journal of Numerical Modelling.* From 1999 to 2009, he has served on the Technical Program Committee of the IEEE MTT-S International Microwave Symposium. He has served as an Associate Editor for the IEEE TRANSACTIONS ON MICROWAVE THEORY AND TECHNIQUES in the area of microwave modeling and CAD from 1999 to 2002 and *International Journal of Electronics and Communications* from 2006 to 2008. He is a Registered Professional Engineer in the province of British Columbia, Canada.

**Lin Gu** (Student Member, IEEE) was born in Ganzhou, Jiangxi, China, in 1998. She received the B.S. degree from Nanchang Hangkong University, Nanchang, China, in 2020. She is currently pursuing the M.S. degree at the School of Electronic Science and Engineering, University of Electronic Science and Technology of China (UESTC), Chengdu, China.

Her research interests include planar hybrid filters, integrated passive device (IPD) filters, and acoustic-wave filters for wireless communication applications.

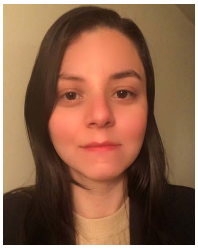

**Deisy Formiga Mamedes** (Member, IEEE) received the B.S. and M.Sc. degrees in electrical engineering from the Federal Institute of Paraiba, João Pessoa, Brazil, in 2016 and 2018, respectively. She is currently pursuing the Ph.D. degree in electrical engineering at the University of Victoria, Victoria, BC, Canada.

She was an Instructor at the Federal Institute of Rio Grande do Norte, Natal, Brazil, from 2017 to 2018, and the Senai College of Paraiba, João Pessoa, from 2018 to 2019. She is currently a Sessional Instructor with the University of Victoria. She has authored/coauthored over 40 technical papers. Her research interests include microwave and millimeter-wave components, modeling of integrated circuits, frequency-selective surfaces, and antennas.